J. Biomed. Eng. Res : 348-354, 2008

A Fast Lower Extremity Vessel Segmentation Method for Large CT Data Sets Using 3-Dimensional Seeded Region Growing and Branch Classification

Dongsung Kim

School of Electronic Engineering, Soongsil University
(Received May 30, 2008. Accepted October 10, 2008)

Abstract

Segmenting vessels in lower extremity CT images is very difficult because of gray level variation, connection to bones, and their small sizes. Instead of segmenting vessels, we propose an approach that segments bones and subtracts them from the original CT images. The subtracted images can contain not only connected vessel structures but also isolated vessels, which are very difficult to detect using conventional vessel segmentation methods. The proposed method initially grows a 3-dimensional (3D) volume with a seeded region growing (SRG) using an adaptive threshold and then detects junctions and forked branches. The forked branches are classified into either bone branches or vessel branches based on appearance, shape, size change, and moving velocity of the branch. The final volume is re-grown by collecting connected bone branches. The algorithm has produced promising results for segmenting bone structures in several tens of vessel-enhanced CT image data sets of lower extremities.

Key words : Image segmentation, bone/vessel segmentation, lower extremity, medium enhanced CT

Ⅰ. INTRODUCTION

Vessels in lower extremity need to be examined for diagnosis of vein anomaly. Although the vessels can be enhanced using contrast enhanced media, it is still very difficult to examine the vessels because bones such as the pelvis, femur, fibula, and tibia block some parts of vessels. Thus, vessel segmentation is necessary for visualization of diagnosis, which is one of the challenging problems in medical image segmentation because of the large variation in gray value, inherent connectivity to bones, and the small size of a vessel.

This paper proposes a complementary approach that segments bones and subtracts them for a clear view of all vessels, including even small isolated vessels and low gray-value vessels. In order to use the segmentation method as a routine diagnosis tool, three challenging problems need to be overcome: leakage due to inherent connection to a vessel, sensitivity due to a threshold, and efficiency to manage several hundred CT images in real time. To achieve these goals, we have developed a fast low extremity segmentation method using 3-dimensional (3D) seeded region growing (SRG) and branch classification.

Corresponding Author : Dongsung Kim
School of Electronic Engineering, Soongsil University
Sangdo-dong 511, Dongjak-Gu, Seoul, Korea 151-743
Tel : +82-2-820-0713 / Fax : +82-2-821-7653
E-mail : dongsung@ssu.ac.kr
This work was supported by the 'Advanced Technology Center Program' grant 10014138 under the Ministry of Knowledge Economy.

Previous research on medical image segmentation focuses mainly on achieving accurate results, and can be classified into three categories[1]: region growing methods[2-4] such as SRG, edge-based methods[5-8] such as snakes, and integrated methods [9-19]. Recently, medical knowledge such as shapes [11-17] and appearance[18-19] has been actively incorporated to achieve more accurate results, and to segment multiple objects[14, 19]. Duncan et al. developed a level set method that provided promising results at the cost of considerable computing time[14]. The necessity of routine clinical use of segmentation makes efficiency another important factor for the segmentation algorithm. Freedman et al.[19] emphasized this issue and developed a fast segmentation algorithm, although it may take several tens of seconds if it is applied to a large image data set of over five hundred. It is necessary to develop an efficient and accurate approach for routine diagnosis.

This paper proposes an efficient algorithm that can produce accurate segmentation results within ten seconds for large image data sets of 512 × 512 × 500~700 slices. The proposed algorithm segments only bones by cutting off a vessel branch

at a junction formed by a bone branch and a vessel branch. Initially, a 3D volume is grown by an SRG method, and junctions of the 3D volume are detected. For all junctions, each branch is classified as either a bone branch or a vessel branch. The classification is determined by appearance, shape, size change, and velocity of a branch. Finally, a bone volume is re-grown from a seed point by collecting only connected bone branches. The details are described in the methods section. Segmentation results performed in several tens of large image data sets taken in routine diagnosis are shown in the results section. This paper is concluded in the final section.

II. MATERIALS AND METHODS

The original 3D SRG[2-3] grows a volume by collecting homogeneous 3D neighbors of voxels in the volume recursively. Although the original method produces a result efficiently, it suffers from leaking to a foreign object because it utilizes only gray value information in deciding homogeneous voxels. A single voxel thick channel can cause a large volume of leakage to a foreign object. The proposed method prevents leaking to a vessel by detecting and cutting a vessel branch. It consists of four modules: growing a 3D volume with an adaptive threshold, detecting junctions, cutting the branch classified as a vessel, and re-growing a 3D volume to collect a bone segmentation result.

A. Growing Initial Volume

Growing a volume is performed by a 3D SRG method, which grows its volume by collecting its homogeneous 3D neighbors iteratively. The six 3D neighbors consist of 4-connected neighbors in the same slice, one in an upper slice, and another in a lower slice. The homogeneity of a neighbor is classified with a gray value. If the value of a neighbor is greater than a threshold, the neighbor is included as the same volume. To accommodate gray-level variability of a bone over different locations, adaptive thresholds are computed. A threshold value playing an important role in segmentation quality is computed by an adaptive threshold method[20]. The method utilizes an estimate of the gradient magnitude around the segmented object edge. The threshold maximizing the average boundary gradient is selected. The maximum average boundary gradient is approximated by selecting a gray value having a maximum average gradient in a bounding box containing an object. The threshold is searched around 1150 of Hounsfield Units (HU) with a margin of 100 HU.

B. Detecting Junctions

When two objects are connected by parts of their attaching surfaces, the surfaces make junctions where the objects meet. A cutting plane above the junction makes two separate regions, while another cutting plane at the junction makes a single region. Thus, a junction can be detected by detecting split regions. If a region at a slice is split into more than two regions at its adjacent slice, those regions form a junction. To distinguish different regions, segmented regions are labeled at each slice.

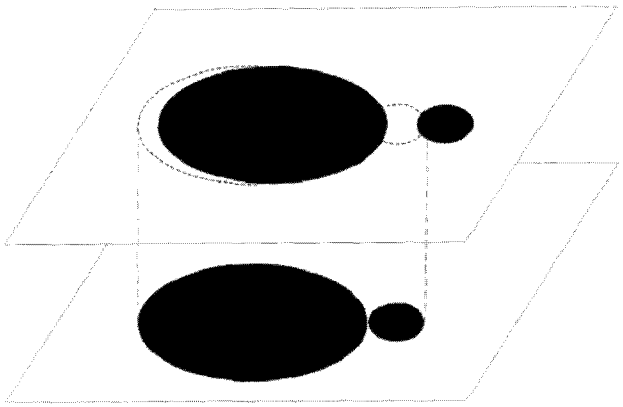

Fig. 1. Junction detection Dotted regions represent projected solid regions from the lower slice

To detect all junctions, every region is checked for whether it has more than two regions at its upper or lower slices. If all pixel points inside a region at a slice have more than two different labels at the adjacent slice, a junction is detected as shown in Figure 1. All junctions have such splitting branches although each split branch may have different shape, direction, and initial position. Once split branch is detected, it is classified into a vessel or a bone based on the criteria described in the following section.

C. Cutting Vessel Branches

Junctions can be generated from three cases: attaching two bones, attaching two vessels, and attaching a bone and a vessel. Whenever a junction is detected, regions are classified as either a bone region or a vessel region. The region classified as a vessel region is marked to prevent a bone from leaking to a vessel branch. The classification of a region is determined by appearance, shape, size change, and velocity of the branch stemming from the region.

A branch, which is a 3D tubular shape, is made with several connected regions along a moving direction. The moving direction can be either an upper direction or a lower direction. When a junction is formed with lower slices, the moving direction is a lower direction. The current system uses four slices to make a branch.

Appearance measures homogeneity of a branch. For computing the homogeneity of a branch, the homogeneity of a region is computed as in Equation 1.

$$\text{homogeneity} = \frac{(\sigma_{Th} - \sigma) + w}{2w} \tag{1}$$

where σ_{Th}, σ, w are deviation threshold, deviation, and window width, respectively. If homogeneity is greater than 1, it is set as 1. If homogeneity is less than 0, it is set as 0. Deviation threshold is 100, and w is 20. Deviation is computed by the absolute difference between the mean value and the gray value of a pixel. The appearance of a branch is an average of the homogeneity of all regions composing a branch as described in Equation 2.

$$AP(b) = \frac{\sum_{k=1}^{n} Homogeneity(k)}{n} \tag{2}$$

where n is number of regions composing a branch.

The shape of a branch measures compactness. For each region, compactness is computed as in Equation 3.

$$Compactness = \frac{8m}{\pi(l^2 + h^2)} \tag{3}$$

where m, l, and h are pixel population, width, and height of a region, respectively. Because a smaller size region of a vessel tends to have a less round shape than a larger size region of a vessel, the compactness of a region is weighted by its size. The shape of a branch is a normalized sum of compactness of all regions as given by Equation 4.

$$Sh(b) = \frac{\sum_{k} Compactness(k) \times W_k}{\sum_{k} W_k} \tag{4}$$

where W_k is a size weighting factor.

The size change of a branch measures area changes of the regions composing the branch. An area change is computed by ratio of the size of a smaller region over that of a larger region and is normalized as in Equation 5.

$$Areachange = \frac{r - w_r}{1 - w_r} \tag{5}$$

where r is ratio of the size of a smaller region over that of a larger region and w_r is an offset value with 0.33. If an area change is less than 0, it is set as 0. The size change of a branch is a normalized sum of area changes, given by Equation 6.

$$SC(b) = \frac{\sum_{k=1}^{n-1} Areachange(k)}{n-1} \tag{6}$$

where n is number of regions composing a branch.

The velocity of a branch is a shift of center points of regions as in Equation 7.

$$shift = \frac{\sqrt{(x_{k+1} - x_k)^2 + (y_{k+1} - y_k)^2}}{\sqrt{P_k / \pi}} \tag{7}$$

where P_k is the population of a region. If the shift is greater than 1, it is set as 1. The velocity of a branch is a sum of shifts, given in Equation 8.

$$V(b) = \sum_{k} shift(k) \tag{8}$$

The classification of a branch utilizes the characteristics of a vessel. A vessel has a tubular shape with homogeneous gray value, in which a size change of cross sections along the center line is small. If a vessel can be segmented as an isolated object, those characteristics can be directly applied for classification. However, segmenting an isolated object is another difficult problem that requires classification. Rather, anatomical knowledge is incorporated to add extra characteristics of a vessel. Vessels are connected to bones at specific locations such as vertebrae, pelvis, etc. For those locations, vessels can fall into two categories in terms of approaching velocity: slow and fast. For a slow approaching case, a vessel can have typical characteristics of shape and size change as described above because an image slice can show the cross section of a vessel along the center line. On the contrary, a vessel with a fast approaching velocity can have different characteristics of shape and size change because an image slice can cut not a perpendicular cross section but a slanted cross section that can produce an elliptical region. To accommodate the two cases, a branch is classified as a vessel if it satisfies either $AP(b) > a \text{ and } SC(b) > c \text{ and } SH(b) > s$ or $V(b) > v \text{ and } AP(b) > a$. The values for the parameters are set as a= 0.6, c=0.6, s= 0.6 and v= 2.

Table 1. Data sets used for evaluation

Data Set	Sex	Number of slice	Thickness (mm)	Spacing (mm)
1	M	674	3.20	1.60
3	M	504	3.20	1.60
4	M	580	3.20	1.60
5	M	874	1.25	1.25
6	M	444	3.00	1.50
7	M	1074	2.00	1.60
8	M	682	3.20	1.00
9	M	1113	2.00	1.00
10	M	1201	2.00	1.00
11	M	1097	2.00	1.00
12	M	1099	2.00	1.00

III. RESULTS

The proposed method was applied to vessel enhanced image data sets composed of about 500 ~ 1200 CT images of size 512 × 512. The evaluation of the method was performed in two groups of data sets. The first data set group consists of eleven image data sets selected to represent ordinary patients and was given at the development of the system. The data sets include lower parts of a body from abdomen to feet. The details of the data sets are summarized in Table 1. It specifies data set number, sex, number of slices, image thickness, and spacing between slices. The second data set group was randomly selected at a hospital when performance evaluation was performed to test robustness of the method and consisted of five patient data sets. All the quantitative analysis was performed with the first data set group, while only subjective evaluation was performed with the second data set group.

The 3D view for Data Set 11, composed of 1097 image slices, is shown in Figure 2-a. It shows bone structures and medium enhanced vessel structures. The segmentation result using a conventional 3D SRG is shown in Figure 2-b. Leaking to vessel structures results in an image containing both bones and vessels. Such leaking comes from vessels attaching to bones such as a vertebra and the pelvis. The attached cases are illustrated with 2D images in Figure 3. The case of attaching to a vertebra is shown in Figure 3-a, while the case of attaching to the pelvis is shown in Figure 3-b. Junctions of those cases are detected, and vessel regions are correctly classified as in Figure 4. The final segmentation results of bone structures and remaining vessel structures are illustrated with 3D views in Figure 5. For Data Set 9 composed of 1113 image slices, 3D views of original data, segmented bone structures, and remaining vessel structures are shown in Figure 6-a, b, and c, respectively. All connected bone structures are successfully segmented, but the two ribs and two patellae are left because they are disconnected from the main bone structure in the CT

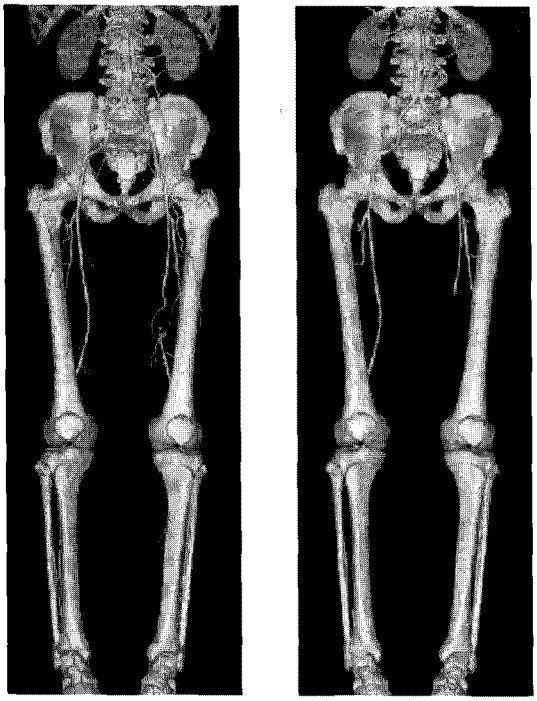

Fig. 2. (a) 3D viewof Data Set 11 (b) SRG result

Fig. 3. (a) Attaching a vessel and a vertebra (b) Attaching vessels and the pelvis

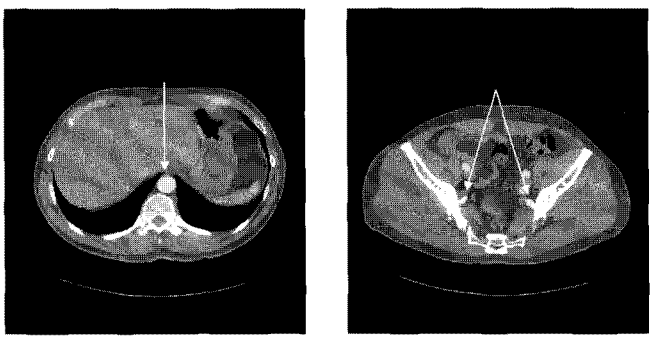

Fig. 4. (a) Classified vessel; pink color (b) Classified vessels; pink color

data set images. The complex shaped vessels are successfully extracted after subtracting the bone structure. The complex shaped vessels are very difficult to extract with a method attempting to segment vessels directly due to the complex structure.

Figure 7-a shows a 3D leg view of Data Set 1, composed of 674 image slices. It contains a large number of isolated vessels that are difficult to segment using conventional methods because the conventional methods utilize the connectivity of an object. On the contrary, the proposed method can segment such isolated vessels using the proposed complementary approach. The result from bone subtraction is shown in Figure 8-b. All isolated vessels are successfully segmented.

Validation of the method is performed quantitatively and qualitatively. The sensitivity, which is a ratio of the number of classified bone branches out of the number of true bone branches, was 100%. The specificity, which is the number of vessel branches classified as bone branches, was 6 branches/ data set. The false positive branches have a non-tubular shape and approach slowly to a bone, which is a characteristic similar to that of a bone branch. Although they can be correctly classified by adjusting parameters, such adjusting reduces sensitivity. Because radiologists preferred to cutoff attached vessels rather than draw a missing bone for routine use, the system is designed to have 100% sensitivity, and provides a one-click interactive tool to cut off a false positive branch. In

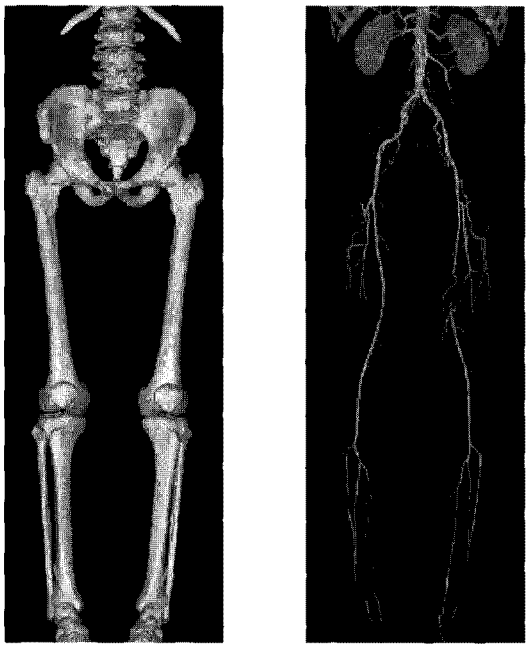

Fig. 5. (a) Bone segmentation (b) Subtracted result

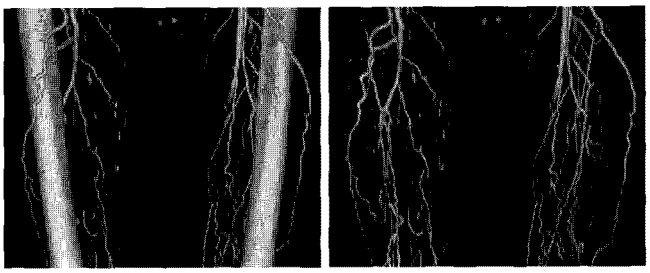

Fig. 7. (a) Bone and vessels (b) Vessel remnants

Fig. 6. (a) 3D view of Data Set 9 (b) Bone segmentation (c) Vessel result

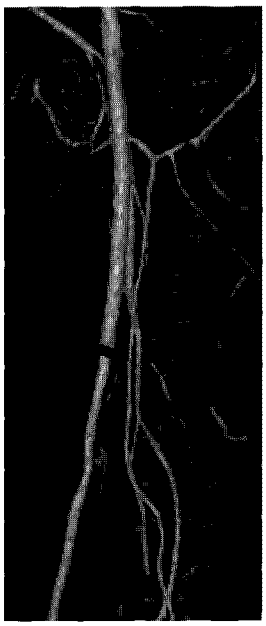

Fig. 8. Vessel Cut off

the validation of the method, classification of true and false branches was performed by a human operator. Qualitative evaluation was also performed for both data set groups by three professors in the radiology department. The results from the first data set group composed of the eleven data sets used in its development were evaluated as very promising. Moreover, five image data sets as the second data set group were randomly selected from patient data sets taken in May 2005 in a university hospital. The data sets were chosen by doctors from patients for diagnosing vessel anomalies of lower extremities, which aims to verify the proposed method for routine use because many methods published in journals actually fails to work in real data sets. The proposed method was evaluated as very promising for routine use. Comparison to a conventional SRG method showed that bone structure leaked to vessels attached to bones in all data sets and produced similar results as Figure 2-b. This comparison is performed because the SRG has a comparable efficiency for routine diagnosis use although more sophisticated methods such as an active shape models can produce more accurate results. However, such a complicated method, we believe, takes much more computing time that prevents the method from being used for routine diagnosis at the current computing power.

The computation time was measured using a Intel Dual Core 2 Duo 2.4GHz processor with 2G main memory. Due to the loading limitations of the visualization software, data sets with more than 700 slices were loaded with even numbered slices. For about 500~700 slices of 512×512 CT images of eleven data sets, the computation time took less than two seconds. Furthermore, removing unnecessary growing to vessels in the first step and the redundant re-growing in the third step will reduce computation time by half.

Separation of attached vessels is necessary for correct segmentation of vessels. When a vessel is attached to a bone, the attached vessel region is segmented as a bone region in the current implementation, although it does not leak over a vessel branch in a junction. Such a vessel region makes a cut-off in a vessel as shown in Figure 9. For recovery of the cut-off, detection and separation of vessels attached to a bone will be studied.

Ⅳ. CONCLUSION

As an alternative approach for segmenting vessels in lower extremity, segmenting and subtracting bones have been implemented. The bone segmentation method has successfully segmented bone structures efficiently for routine use. The segmented bone structures are subtracted to achieve vessel structures that can have a very complex shape and can contain a large number of isolated vessel segments. The segmentation method prevents leaking to a vessel structure by detecting a junction and cutting a vessel branch. To classify a vessel branch, appearance, shape, size change, and velocity of a branch are computed. The classification is performed only at junctions while a 3D volume is growing with an efficient SRG, which makes the segmentation method efficient. Separating vessels attached to bones will be studied.

REFERENCES

[1] D. Duncan and N. Ayache, "Medical Image Analysis: Progress over Two Decades and the Challenges Ahead," *IEEE Trans. on the Pattern Analysis and Machine Intelligence*, vol. 22, no. 1, pp. 85-106, January 2000.

[2] R. Adams and L. Bischof, "Seeded region growing," *IEEE Trans. on the Pattern Analysis and Machine Intelligence*, vol. 16, no. 6, pp. 641-647, June 1994.

[3] T.Kapur, W. Grimson, W. Wells. III, and R. Kinis, "Segmentation of brain tissue from magnetic resonance images," *Medical Image Analysis*, vol. 1, no. 2, pp. 109-127, 1996.

[4] A. Elmoutaouakkil, F. Peyrin, J. Elkafi, A. Laval-Jeantet, "Segmentation of cancellous bone from high-resolution computed tomography images: influence on trabecular bone measurements," *IEEE Trans. on medical imaging*, vol. 21, no. 4, pp. 354-362, December 1996.

[5] M.Kass, A. Witkin, and D. Terzopoulos, "Snakes: active contour models," *International Journal of Computer Vision*, vol. 1, no. 3, pp. 312-331, 1988.

[6] L.Cohen and I. Cohen, "Finite-element methods for active contour models and balloons for 2-d and 3-d images," *IEEE Trans. on the Pattern Analysis and Machine Intelligence*, vol. 15, no. 11, pp. 1,131-1,147, November 1993.

[7] T.B. Sebastian, H. Tek, J.J. Crisco, S.W. Wolfe, and B.B. Kimia, "Segmentation of carpal bones from 3D CT images using skeletally coupled deformable models," MICCAI'98, LNCS 1496, pp1184-1194, 1998

[8] W.Barrett and N. Mortensen, "Interactive live-wire boundary extraction," *Medical Image Analysis*, vol. 1, no. 4, pp. 331-341, September 1997.

[9] C.Chu and J.K. Aggarwal, "The integration of image segmentation maps using region and edge information," *IEEE Trans. on the Pattern Analysis and Machine Intelligence*, vol. 15, no. 12, pp. 1241-1252, December 1993.

[10] A. Chakraborty, L. Staib, and J. Duncan, "Deformable boundary finding in medical images by integrating gradient and region information," *IEEE Trans. on medical imaging*, vol. 15, no. 6, pp. 859-870, December 1996.

[11] M.E. Leventon, W.E.L. Grimson, and O. Faugeras, "Statistical shape Influence in Geodesic Active Contours," *Proc. Computer Vision and Pattern Recognition (CVPR)* pp. 316-323, 2000.

[12] X. Zeng, L.H. Staib, R.T. Shultz and J.S. Duncan, "Segmentation and measurement of the cortex from 3-D MR images using

coupled-surface propagation," *IEEE Trans. Med. Imag.*, vol. 18, pp. 927-937, Oct. 1999.

[13] M. Xu, P.M. Thompson, and A.W. Toga, "An adaptive level set segmentation on a triangulated mesh," *IEEE Trans. Med. Imag.*, vol. 23, pp. 191-201, Feb. 2004.

[14] J. Yang, H. Staib, and J.S. Duncan, "Neighbor-constrained segmentation with level set based 3-D deformable models." *IEEE Trans. Med. Imag.*, vol. 23, pp. 940-948, Aug. 2004.

[15] A. Tsai, A. Yezzi, W. Wells, C. Tempany, D. Tucker, A. Fan, E. Grimson, and A. Willsky, "A shape based approach to curve evolution for segmentation of medical imagery," *IEEE Trans. Med. Imag.*, vol. 22, no. 2, Feb. 2003.

[16] M.B. Cuadra, C. Pollo, A. Bardera, O. Cuisenarie, J.G. Villemure, and J.P. Thiran, "Atlas-based segmentation of pathological MR brain images using a model of lesion growth," *IEEE Trans. Med. Imag.*, vol. 23, pp.1301-1314, Oct. 2004.

[17] J. Ehrhardt, H. Handels, T. Malina, B. Strathmann, W. Plötz, S.J. Pöppl, "Atlas-based segmentation of bone structures to support the virtual planning of hip operations," *International Journal of Medical Informatics*, vol. 64, pp439-447, 2001.

[18] T. Cootes and C. Taylor, "Statistical models of appearance for medical image analysis and computer vision," *Proc. SPIE medical Imaging 2001*, vol. 4322, pp 236-248, Jul. 2001.

[19] D. Freedman, R.J. Radke, T. Zhang, Y. Jeong, D.M. Lovelock, and G. T.Y. Chen, "Model-based segmentation of medical imagery by matching distributions," *IEEE Trans. Med. Imag.*, vol. 24, pp.281-292, Mar. 2005.

[20] K.R. Castleman, Digital Image Processing. Upper Saddle River NJ: Prentice Hall, 1996